J. Fluid Mech. (1986), *vol.* 163, *pp.* 405–423
Printed in Great Britain

Flow of axisymmetric red blood cells in narrow capillaries

By T. W. SECOMB,
Departments of Physiology and Mathematics, University of Arizona, Tucson, Arizona 85724

R. SKALAK, N. ÖZKAYA
Bioengineering Institute, Columbia University, New York, NY 10027

AND J. F. GROSS
Department of Chemical Engineering, University of Arizona, Tucson, Arizona 85721

(Received 19 March 1985 and in revised form 16 July 1985)

Flow of red blood cells along narrow cylindrical vessels, with inside diameters up to 8 μm, is modelled theoretically. Axisymmetric cell shapes are assumed, and lubrication theory is used to describe the flow of the suspending fluid in the gaps between the cells and the vessel wall. The models take into account the elastic properties of the red blood cell membrane, including its responses to shear and bending. At moderate or high cell velocities, about 1 mm/s or more, the membrane stress may be approximated by an isotropic tension which is maximal at the nose of the cell and falls to zero at the rear. Cell shape and apparent viscosity are then independent of flow rate. At lower flow velocities, membrane shear and bending stresses become increasingly important, and models are developed to take these into account. Apparent viscosity is shown to increase with decreasing flow rate, in agreement with previous experimental and theoretical studies.

1. Introduction

Blood flow in microvessels (with diameters of about 100 μm or less) presents intricate problems in fluid and solid mechanics, and present theoretical understanding is limited, despite the physiological importance of the phenomena involved. For example, the apparent viscosity of blood in narrow tubes is substantially lower than the bulk viscosity (the Fahraeus–Lindqvist effect). Also, the haematocrit (volume fraction of red blood cells) is reduced in microvessels compared to systemic values. This is the result of several factors including the difference between mean-red-cell and bulk-flow velocities (the Fahraeus effect). Early theoretical work in this area was reviewed by Whitmore (1968) and Gross & Aroesty (1972), and the literature has continued to expand. A number of studies (e.g. Thomas 1962; Gupta, Nigam & Jaffrin 1982) have modelled blood rheology in microvessels with a wide range of diameters by extending continuum models to include the effects of cell-free or cell-depleted regions near the vessel walls. These studies usually involve one or more parameters which must be obtained empirically by fitting to experimental data. A more fundamental approach is to predict rheological properties starting from known mechanical properties of individual blood cells. This approach is particularly suitable for modelling flow in capillaries with diameters less than about 8 μm, in which red blood cells frequently travel in single file, each cell almost filling the lumen.

The basic mechanical properties of the human red blood cell have been much studied in recent years, and they are now fairly well established. In fact, the human red cell provides an unusual instance in which mechanical properties of a biological system are known in detail at the cellular level. Problems of blood flow in microvessels are therefore particularly well suited to a theoretical approach. In this study we develop theories for blood flow in narrow capillaries which exploit this information about the red cell.

Starting with the work of Barnard, Lopez & Hellums (1968) and Lighthill (1968), most theoretical studies of blood flow in narrow capillaries have rested on two key approximations. Firstly, the fact that individual cells almost fill the lumen has suggested the use of lubrication theory to describe the fluid flow in the narrow gaps between the cells and vessel walls. Earlier, Bretherton (1961) used this theory in studying the motion of bubbles in tubes. In lubrication theory, the equations of fluid motion are simplified by the neglect of inertia and by the assumption that the thickness of the gap between the two surfaces is small compared with the other dimensions involved. Secondly, microscopic observations have shown that red blood cells in narrow capillaries may have approximately axisymmetric shapes, and the deformed cell geometry has been assumed to be axisymmetric. We use both these approximations in this study.

Some studies have been based on different assumptions. Zarda, Chien & Skalak (1977*a*) also assumed axisymmetric geometry in analysing capillary flows at low velocities, but used a finite-element method which did not require the narrow-gap approximation of lubrication theory. The effects of asymmetry in cell shapes were investigated by Secomb & Skalak (1982) using a two-dimensional lubrication-theory model.

In §2 we discuss the mechanical properties of red blood cells, and in §3 we formulate the problem. Sections 4 and 5 are devoted to solutions in which successively more details of the red cell's mechanical response are incorporated.

2. Mechanical properties of the red blood cell

The original models of Lighthill and Barnard *et al.* differed in their assumptions about the mechanical properties of individual red blood cells, but neither was very satisfactory in this regard. Lighthill (1968) assumed that the undeformed cell shape near the wall is parabolic, and the deformation of the cell is proportional to the local pressure. This approximation may be applicable for solid elastic or viscoelastic cells (such as white blood cells), but is not well suited to describing the mechanics of a fluid-filled sac (the red cell). Subsequent developments of this model (Fitz-Gerald 1969; Lomen & Gross 1977; Vann & Fitz-Gerald 1982) used the same approximation to the mechanical properties of the cell. The case of solid elastic spheres was treated by Tözeren & Skalak (1979).

In the model developed by Barnard *et al.* (1968) the cell is represented as a flexible circular sheet which is deformed in flow into a hollow 'thimble' shape with isotropic tension acting in the cell membrane, maximal tension occurring at the 'nose' of the cell. The stress in the sheet is approximated by an isotropic in-plane tension. Observed cell shapes are in fact much less concave at the rear than this model suggests, and in a subsequent study (Lin, Lopez & Hellums 1973) essentially the same analysis was used but the cell was represented as a solid bullet-like shape with isotropic tension acting in the cell membrane.

The basic mechanical properties of red blood cells are fairly well established (Skalak

1976). A thin membrane surrounds the cytoplasm, which is considered to be an incompressible Newtonian fluid. The membrane exhibits viscoelastic properties, but under steady conditions only the elastic deformation needs to be considered. The elastic shear modulus of the membrane (4.2×10^{-3} dyn/cm; Chien *et al.* 1978) is several orders of magnitude lower than the modulus of isotropic dilatation (about 500 dyn/cm) and so the membrane shears readily but resists area changes. Also, bending resistance is small unless very small radii of curvature are involved; the bending modulus is estimated to be 1.8×10^{-12} dyn cm (Evans 1983).

An axisymmetric red blood cell subjected to steady external forces assumes a configuration in which the external forces are balanced by stresses induced within the membrane and cytoplasm. The character of the membrane stresses depends on the magnitude of the applied forces. Relatively small external forces will generally be balanced by a combination of tension, shear and bending stresses in the membrane. When the fluid stress on the cell is increased, large strains are required to generate corresponding increases in shear stress, and sharp curvatures are required to generate correspondingly large bending stresses. In an axisymmetric flow configuration, the magnitude of shear strains possible in an intact cell without membrane dilatation is limited. On the other hand, large isotropic tensions may be generated by small membrane dilatation. This suggests that such a highly stressed cell tends to assume a configuration in which external fluid forces are balanced primarily by isotropic membrane tension, except possibly at localized regions of high curvature. The dominant membrane stress over most of the cell surface will then be isotropic tension, if the cell velocity is sufficiently large. Lin *et al.* (1973) developed a self-consistent model in which isotropic membrane tension is assumed and bending stresses are neglected, which has been further elaborated by Secomb & Gross (1983) and here in §4.

Membrane shear and bending forces become increasingly important at lower cell velocities, and the membrane tension is no longer approximately isotropic. In analysing the effects of shear and bending elasticity, we use constitutive relations proposed by Evans & Skalak (1980, pp. 77, 109), as they apply to an axisymmetric membrane shell. Arclength s, measured from the nose of the cell, describes the position on the membrane. Other variables, indicated in figure 1, are $r(s)$, distance from the axis; $\theta(s)$, angle between the normal to the membrane and the axis; $k_s(s)$ and $k_\phi(s)$, membrane curvatures; $m_s(s)$ and $m_\phi(s)$, bending moments; $t_s(s)$ and $t_\phi(s)$, membrane tension; and $q_s(s)$, shear force per unit length. The subscript s denotes components in a plane containing the axis, while ϕ denotes azimuthal components. Because of the high modulus of dilatation, we treat the membrane as incompressible in a two-dimensional sense (i.e. the deformation is locally area preserving). In this case the mean tension $t_m(s)$ is analogous to the hydrostatic pressure in incompressible fluid flow. Then the components of tension are

$$t_s = t_m + t_d \quad \text{and} \quad t_\phi = t_m - t_d, \tag{2.1}$$

where

$$t_d = \tfrac{1}{2}\kappa(\lambda^2 - \lambda^{-2}), \tag{2.2}$$

κ is the shear modulus of the membrane and $\lambda = ds/ds_0 = r_0/r$ is the extension ratio of a membrane element in the s direction relative to the unstressed shape. The subscript 0 denotes the unstressed state. The bending moment is assumed to be isotropic and proportional to the increase in total curvature of the surface (Evans & Skalak 1980):

$$m_s = m_\phi = B[(k_s + k_\phi) - (k_s + k_\phi)_0], \tag{2.3}$$

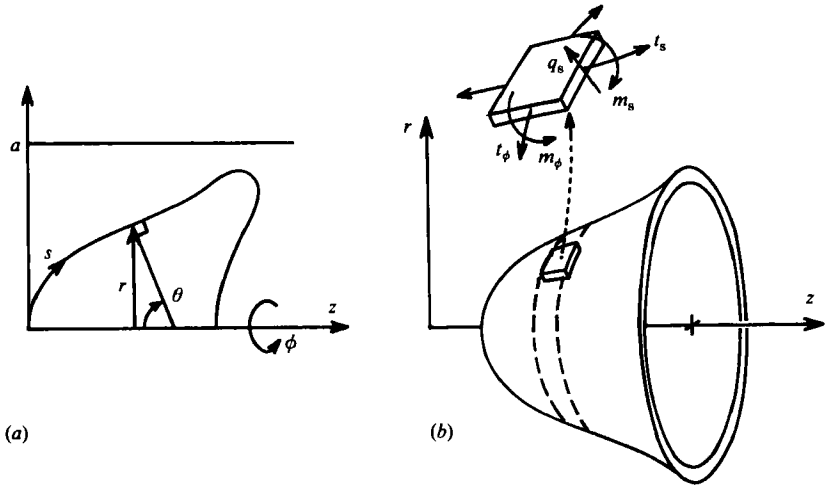

FIGURE 1. (*a*) Variables describing the geometry of an axisymmetric shell. (*b*) Stress resultants in an element of an axisymmetric shell.

where the principal radii of curvature are given by

$$k_s = \frac{d\theta}{ds} \quad \text{and} \quad k_\phi = \frac{\sin\theta}{r}, \tag{2.4}$$

and B is the bending modulus. A more general model for the bending response is given by Skalak (1976) and Zarda *et al.* (1977*a*), including (2.3) as one possibility.

For axisymmetric shells, the equations of mechanical equilibrium are given by Timoshenko (1940). The hydrodynamic loading on the cell in this instance consists of the hydrostatic pressure difference $p(s)$ between the external and internal fluids and the viscous shear stress $\tau(s)$ due to the external fluid. (The viscous normal stress vanishes because the fluid velocity in a frame moving with the cell is zero at the cell surface and the flow is incompressible.) The equations for equilibrium of normal stress, tangential stress and bending moments in the membrane are respectively:

$$\frac{1}{r}\frac{d(rq_s)}{ds} = p - k_s t_s - k_\phi t_\phi, \tag{2.5}$$

$$\frac{1}{r}\frac{d(rt_s)}{ds} = \frac{t_\phi \cos\theta}{r} + k_s q_s - \tau, \tag{2.6}$$

$$\frac{1}{r}\frac{d(rm_s)}{ds} = \frac{m_\phi \cos\theta}{r} - q_s. \tag{2.7}$$

In this formulation, we have assumed that the red cell has an unstressed shape which is axisymmetric and that the same axis pertains to the cell in the final shape. The question of the existence and nature of an unstressed shape for the red-cell membrane is not settled (Fischer *et al.* 1981*a*, *b*). Zarda *et al.* (1977*a*) assumed that the cell was unstressed with respect to both shear and bending in a biconcave disk shape, coaxial with the vessel. Here we assume that the cell is unstressed in a spherical shape with the same surface area as the cell. The consequences of these assumptions are discussed in §6. The density of red cells differs only slightly from that of plasma, and buoyancy effects are neglected here.

3. Formulation using lubrication theory

3.1. *Governing equations*

In applying lubrication theory, we assume that the typical width of the gap between the cell and the vessel wall is small compared to the lengthscale of the gap. Generally, this implies that the gap is small compared to the vessel radius, and suggests the possibility of using two-dimensional lubrication theory to describe the flow in the neighbourhood of the wall. However, it is not necessary to make this approximation, and we shall show that using the axisymmetric form of lubrication theory yields significantly more accurate results in certain cases. At this stage, therefore, we make no explicit assumption regarding the smallness of the gap relative to the vessel radius.

Typical cell shapes are rounded at the leading end. In this region the gap is not uniformly narrow, and lubrication theory no longer strictly applies. The pressure gradient is, however, small in this region compared to its values in the narrow gap (see §4.2), and so the error in the calculated overall pressure drop resulting from applying lubrication theory uniformly along the whole length of the cell is small.

In the cylindrical coordinates (σ, ϕ, z) moving with the cell, the flow is steady and the pressure $p(z)$ in the gap depends only on z, the axial position (figure 1*b*). The axial velocity $u(\sigma, z)$ satisfies:

$$\frac{\mu}{\sigma}\frac{\partial}{\partial\sigma}\left[\sigma\frac{\partial u}{\partial\sigma}\right] = \frac{\mathrm{d}p}{\mathrm{d}z}, \tag{3.1}$$

with boundary conditions $u = 0$ on the cell surface $\sigma = r(z)$, and $u = u_0$ at the vessel wall $\sigma = a$, where u_0 is the cell velocity and a is the vessel radius. The volume flow of fluid relative to the cell is known as the 'leakback' and is independent of z. The leakback q_0 per unit circumference is given by

$$q_0 = \int_r^a \frac{u(\sigma, z)\,\sigma}{a}\,\mathrm{d}\sigma. \tag{3.2}$$

Equations (3.1) and (3.2) may be solved for the pressure gradient in terms of $r(z)$ and q_0 (Tözeren & Skalak 1978):

$$\frac{\mathrm{d}p}{\mathrm{d}z} = g(r) = \frac{16\mu}{a^2-r^2}\left[u_0\left[\frac{a^2}{2}+\frac{a^2-r^2}{4\log(r/a)}\right]-aq_0\right]\left[a^2+r^2+\frac{a^2-r^2}{\log(r/a)}\right]^{-1}. \tag{3.3}$$

The shear stress acting on the cell surface is then given by

$$\tau(r) = \tfrac{1}{4}g(r)\left[\frac{a^2-r^2}{r\log(r/a)}+2r\right]-\frac{\mu u_0}{r\log(r/a)}. \tag{3.4}$$

The complete system of differential equations is obtained by combining the equations governing the elastic response and mechanical equilibrium of the membrane (2.1)–(2.7) with the equations of lubrication theory (3.1)–(3.4). It is convenient to use arclength s as the independent variable:

$$\frac{\mathrm{d}r}{\mathrm{d}s} = \cos\theta, \tag{3.5}$$

$$\frac{\mathrm{d}\theta}{\mathrm{d}s} = k_{\mathrm{s}}, \tag{3.6}$$

$$\frac{\mathrm{d}k_{\mathrm{s}}}{\mathrm{d}s} = \frac{\sin\theta\cos\theta}{r^2}-\frac{\cos\theta\,k_{\mathrm{s}}}{r}+\frac{q_{\mathrm{s}}}{B}, \tag{3.7}$$

$$\frac{dq_s}{ds} = k_s t_s + \frac{[t_s - \kappa(\lambda^2 - \lambda^{-2})]\sin\theta}{r} + p - \frac{q_s \cos\theta}{r}, \tag{3.8}$$

$$\frac{dp}{ds} = g(r)\sin\theta, \tag{3.9}$$

$$\frac{dt_s}{ds} = -\frac{\kappa(\lambda^2 - \lambda^{-2})\cos\theta}{r} - k_s q_s - \tau(r). \tag{3.10}$$

It may be shown using (3.5), (3.6), (3.8) and (3.10) that the net axial force on the particle vanishes:

$$\int_0^{s_1} 2\pi r(p\cos\theta + \tau\sin\theta)\,ds = 0, \tag{3.11}$$

where s_1 is the total arclength, as long as $rq_s \to 0$ as $r \to 0$. This is the so-called 'zero drag' condition. The other boundary conditions are that r and θ vanish on the axis, and that the surface area and volume are prescribed.

Note that the shape of a freely suspended red blood cell may be calculated by setting $\tau = 0$ and $p =$ constant in the system (3.5)–(3.10). This provides an alternative approach to the finite-element method of Zarda *et al.* (1977*b*).

3.2. *Calculation of apparent viscosity and Fahraeus effect*

The analyses in §§4 and 5 will provide estimates of the pressure drop Δp across the red cell and the leakback q_0. From these we may calculate two key rheological parameters: the reduction of haematocrit due to the Fahraeus effect, and the apparent viscosity. Because the red-cell velocity u_0 is higher than the mean bulk velocity $\bar{u}$, the haematocrit H_T within the microvessel is lower than the discharge haematocrit H_D which would result if the blood emerging from the microvessel were collected, and they are related by (Sutera *et al.* 1970):

$$\frac{H_T}{H_D} = \frac{\bar{u}}{u_0}. \tag{3.12}$$

The reduction in haematocrit is therefore given by

$$\frac{H_T}{H_D} = 1 - \frac{2q_0}{au_0}. \tag{3.13}$$

In the lubrication models, effects of interactions between cells are assumed negligible. The apparent viscosity μ_{app} therefore depends linearly on the haematocrit, and is expressed in terms of a parameter K_T, the apparent intrinsic viscosity, where

$$\mu_{app} = \mu(1 + K_T H_T). \tag{3.14}$$

If it is assumed that the pressure drop in the regions between cells is given by the Poiseuille formula, then

$$K_T = \frac{\pi a^2}{V}\left[\frac{\Delta p\, a^2}{8\mu(u_0 - 2q_0/a)} - l\right], \tag{3.15}$$

where l is the length of the cell. These assumptions are justified on the basis of studies of the 'bolus' flow in the region between cells. Lew & Fung (1969) and Papenfuss & Gross (1982) calculate the pressure drop in the region between two cylindrical particles moving along a vessel. Both studies demonstrate a pressure drop additional to the Poiseuille estimate in the fluid adjacent to each particle, which is independent

	$P_0 = ap_0/\mu u_0$		
λ'	Wang & Skalak (1969) (series expansion)	Axisymmetric lubrication theory (numerical)	Two-dimensional lubrication theory (closed-form)
0.600	6.9836	6.8778	9.8266
0.700	9.8601	9.7153	12.3927
0.800	15.7262	14.8492	17.2289
0.900	28.4832	27.8270	29.7785
0.950	—	48.1138	49.6663
0.980	—	91.2154	92.2876
0.990	—	141.5370	142.3033
0.995	—	213.8301	214.3655
0.998	—	358.6905	358.9627

TABLE 1. Comparison of estimates of the dimensionless driving pressure P_0 for rigid spherical particles. λ' is the ratio of particle diameter to tube diameter.

of the particle spacing if the spacing is more than one vessel diameter. The extra pressure drop is conveniently expressed as an equivalent length l_a via Poiseuille's law. The calculations of Papenfuss & Gross (1982), in which the particle radius equals the vessel radius a, give $l_a \simeq 0.75a$. Lew & Fung (1969) assume a particle radius of $0.9a$ and their results imply $l_a \simeq 0.5a$. In the latter study, there was a leakback $q_0 = 0.05$, suggesting that l_a decreases with increasing leakback. The blunt-ended particle filling the vessel is an extreme case and gives an upper limit to this effect. The additional pressure drop near a hemispherical-ended particle is probably considerably less. These arguments indicate that the additional pressure drop in the fluid beyond the ends of the cell can be neglected in our calculations.

3.3. *Rigid particles and spheres*

Depending on the assumptions made, a number of different approaches are available to solve the system of equations given in §3.1. If rigid axisymmetric particles with given geometries are considered, (3.3) and (3.4) and the zero-drag condition (3.11) are sufficient to solve the problem.

The application of the zero-drag condition requires some caution. This condition is used to determine the leakback q_0, which is an unknown parameter in (3.3). According to the narrow-gap assumption, $\sin\theta \simeq 1$ and $\cos\theta \simeq 0$ in the lubrication region. But, if these approximations are made in (3.11), the resulting simplified zero-drag expression may yield very inaccurate results for q_0, and hence the pressure drop (Lighthill 1968; Tözeren & Skalak 1978). Because large pressures may occur in the gap, the term $p\cos\theta$ is not negligible. Similarly, retention of the term $\sin\theta$ in (3.9) yields improved accuracy, even though its neglect would be consistent with the lubrication approximation. This point may be illustrated by considering spherical particles. Wang & Skalak (1969) studied the viscous flow of a line of rigid spheres in a cylindrical tube, giving series expansions for the exact solutions. The results of Wang & Skalak are expressed in table 1 in terms of dimensionless pressure drop per particle. The estimates for pressure drop from axisymmetric lubrication theory, taking the $\sin\theta$ term into account, agree closely with the results of Wang & Skalak (1969), even for values of λ', the ratio of particle diameter to tube diameter, as low as 0.6.

Table 1 also indicates that the two-dimensional approximation to lubrication theory, obtained by replacing the first term of (3.1) by $\mu\partial^2 u/\partial\sigma^2$, yields quite accurate results for spheres with diameter ratios of 0.9 or more. In this approximation, closed-form solutions are available for spheres and for certain other axisymmetric shapes such as cylindrical particles with flat or hemispherical ends. Details are given by Özkaya (1985). For values of λ' between 0.6 and 0.8, axisymmetric lubrication theory is seen to yield significantly more accurate results than the two-dimensional form, and was therefore used in most of the calculations reported here.

These results suggest that carefully formulated axisymmetric lubrication theory can yield useful results even for diameter ratios substantially less than one. In the case of more elongated particle shapes, lubrication theory should yield results at least as accurate as those obtained for spherical particles with the same diameter ratio, since the ratio of gap width to gap length is then smaller for more elongated particles.

4. Isotropic membrane tension: the high-velocity limit

4.1. *Formulation in the high-velocity limit*

In this section it is shown that the governing equations admit solutions in which the fluid-mechanical stresses acting on the cell are balanced solely by isotropic tension within the cell membrane, and in which membrane shear and bending resistance are neglected. As mentioned earlier, this corresponds to a limiting solution at high cell velocities. The conditions under which this solution can be considered a valid approximation will be discussed later.

If bending resistance is neglected, (3.5)–(3.10) take a simplified form. The membrane cannot support an out-of-plane shear force ($q_s = 0$), and so (3.7) is redundant and (3.8) reduces to an algebraic equation for k_s. The resulting equations are:

$$\frac{dr}{ds} = \cos\theta, \tag{4.1}$$

$$\frac{d\theta}{ds} = -\frac{p}{t_s} - \frac{\sin\theta}{r}\left[1 - \frac{\kappa(\lambda^2 - \lambda^{-2})}{t_s}\right], \tag{4.2}$$

$$\frac{dp}{ds} = g(r)\sin\theta, \tag{4.3}$$

$$\frac{dt_s}{ds} = -\tau(r) - \frac{\kappa(\lambda^2 - \lambda^{-2})\cos\theta}{r}. \tag{4.4}$$

The further simplification of neglecting membrane shear elasticity is achieved by setting $\kappa = 0$. This system becomes singular when $t_s = 0$, allowing the possibility of a cusp with infinite curvature. Such a cusp is expected at the trailing edge of the cell. In our calculations we have not integrated through the cusp numerically; instead the rear concavity is approximated with a spherical segment.

4.2. *Asymptotic solution for small gaps*

The governing equations can be further simplified if the additional assumption is made that the gap is narrow compared with the vessel *radius* over most of its length. In this case the leakback is correspondingly small compared with the total flow, and we introduce a parameter

$$\epsilon = \frac{2q_0}{au_0} \ll 1, \tag{4.5}$$

and a scaled gap width h where

$$r = a(1-\epsilon h). \tag{4.6}$$

Then the pressure gradient and shear stress are approximately as given by two-dimensional lubrication theory (cf. Lighthill 1968):

$$g = 6\mu u_0 (a\epsilon h)^{-2}(1-h^{-1}+O(\epsilon h)), \tag{4.7}$$

and

$$\tau = \mu u_0 (a\epsilon h)^{-1}(3h^{-1}-2+O(\epsilon h)). \tag{4.8}$$

In this limit, two special solutions to (4.1)–(4.4) may be deduced. One solution (region II in figure 2*a*) corresponds to a cylinder nearly filling the vessel cross-section:

$$\theta = \tfrac{1}{2}\pi, \quad r = r_c, \quad p = g(r_c)(s-s_d) \quad \text{and} \quad t_s = -r_c p, \tag{4.9}$$

where $\tau(r_c) = r_c g(r_c)$, and the membrane tension vanishes when $s = s_d$. Equations (4.7) and (4.8) show that

$$h = 1+O(\epsilon) \quad \text{when} \quad r = r_c. \tag{4.10}$$

The pressure (p) and membrane tension (t_s) are therefore large at the upstream end of this region, both being of order ϵ^{-1}. If we now suppose that pressure and tension of this order are transmitted into a second region in which $h \gg 1$, and where, as (4.7) and (4.8) show, the pressure gradient and shear stress are much smaller, then p and t_s may be approximated by constants in this second region. The resulting solution is:

$$\theta = \frac{s}{r_0}, \quad r = r_0 \sin\theta, \quad p = -p_0 \quad \text{and} \quad t_s = t_{s0}, \tag{4.11}$$

where $0 \leqslant s < \frac{1}{2}\pi r_0$ and $r_0 = 2t_{s0}/p_0$, corresponding to a hemisphere with its pole on the axis.

An overall asymptotic solution for small gaps is obtained by matching the hemisphere (region I) to the cylinder (region II) through a relatively short transition region (region III) as shown in figure 2(*a*). In region III the governing equations (4.1)–(4.4) reduce to:

$$\frac{\mathrm{d}h}{\mathrm{d}s} = -\frac{\theta'}{a\epsilon}, \tag{4.12}$$

$$\frac{\mathrm{d}\theta'}{\mathrm{d}s} = \frac{p}{t_s}+\frac{1}{a}, \tag{4.13}$$

$$\frac{\mathrm{d}p}{\mathrm{d}s} = \frac{6\mu u_0}{a^2\epsilon^2}(h^{-2}-h^{-3}), \tag{4.14}$$

$$\frac{\mathrm{d}t_s}{\mathrm{d}s} = -\frac{\mu u_0}{a\epsilon}(3h^{-2}-2h^{-1}), \tag{4.15}$$

where $\theta' = \frac{1}{2}\pi-\theta \ll 1$. The tension is almost constant in regions I and III so we replace t_s by t_{s0} in (4.13). We introduce an inner coordinate

$$\zeta = \epsilon^{-1}\left(\frac{t_{s0}}{\mu u_0}\right)^{-\frac{1}{3}}\frac{s-s_m}{a}, \tag{4.16}$$

where $h(s_m) = \frac{3}{2}$, and let $h = f(\zeta)$. Then (4.12)–(4.14) give

$$f''' = 6(f^{-3}-f^{-2}). \tag{4.17}$$

The boundary conditions, $f' \to 0$ as $\zeta \to \infty$ and $f(0) = \frac{3}{2}$, uniquely determine $f(\zeta)$, and

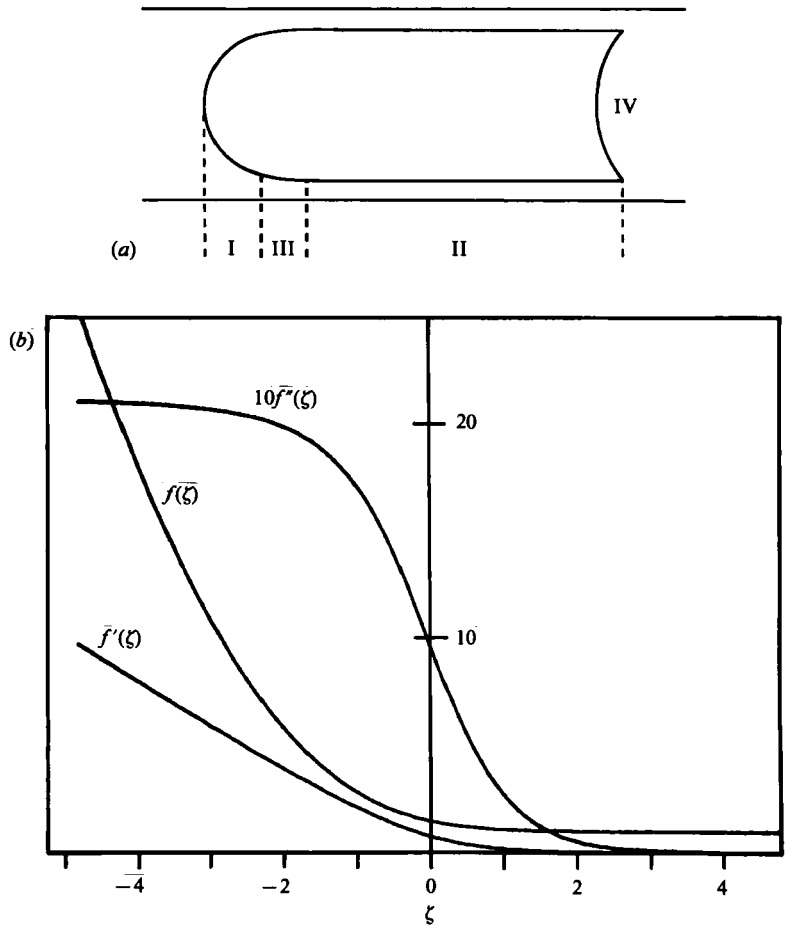

FIGURE 2. Asymptotic model for small gaps. (*a*) Sketch showing regions I–IV of the asymptotic solution. (*b*) The function $f(\zeta)$ and its derivatives.

numerical solution (see figure 2*b*) shows that f'' approaches $k_0 \simeq 2.123$ as $\zeta \to -\infty$. Also,

$$p = -t_{s0}/a\,[1 + (t_{s0}/\mu u_0)^{-\frac{2}{3}} f''(\zeta)/\epsilon], \tag{4.18}$$

and since $p \to -p_0$ as $\zeta \to -\infty$ to match with region I and $p_0 = 2t_{s0}/a$ to leading order, it follows that

$$t_{s0} = \mu u_0 (\epsilon/k_0)^{-\frac{3}{2}} \quad \text{and} \quad p_0 = 2\mu u_0/a\,(\epsilon/k_0)^{-\frac{3}{2}}. \tag{4.19}$$

The asymptotic cell shape is completed by considering the tail region, region IV. The membrane tension falls to zero at $s = s_d$, and the curvature may be infinite, giving a cusp. Beyond this point fluid-mechanical stresses are negligible, so the tension is zero throughout the tail region. The upstream hydrostatic pressure is transmitted into the interior of the cell, and so $p_0 = \Delta p$, where Δp is the pressure drop driving the cell. The shape of the membrane is therefore arbitrary in region IV, subject only to the surface area and volume constraints, and does not affect the solution in the other regions.

An estimate of ϵ can be obtained if the length of the cylindrical region II is known, say γa where $\gamma \gg 1$. Then (4.15) shows that $t_{s0} \simeq \mu u_0 \gamma/\epsilon$ and so

$$\epsilon = k_0^3 \gamma^{-2}. \tag{4.20}$$

The lengthscales of regions I, II and III are therefore a, $a\epsilon^{-\frac{1}{3}}$ and $a\epsilon^{\frac{1}{3}}$ respectively, when the gap width is of order $a\epsilon$. Actual values of γ are restricted by the fixed surface area of the cell. In fact $\gamma < 10$ for normal red blood cells and (4.20) shows that ϵ is not generally small. This asymptotic theory is therefore unsuitable for quantitative predictions. However, it allows us to draw several conclusions about the dynamics of axisymmetric red-cell motion at high velocities in narrow capillaries. (i) The cell is bullet-shaped with a hemispherical nose. (ii) The pressure in the lubrication layer varies monotonically, in sharp contrast to its behaviour in the case of spherical particles. There is a sharp rise in pressure in the transition region near the nose, and a gradual rise along the remainder of the cell's length. (iii) The gap width along most of the length of the cell is constant and is determined by the fluid mechanics of the transition region and the length of the cell. (iv) The apparent viscosity is independent of cell velocity when the velocity is high, since Δp is proportional to u_0.

4.3. *Numerical solution*

The equations (4.1)–(4.4) with $\kappa = 0$ are first rewritten in dimensionless form and then integrated numerically. The results confirm the above qualitative conclusions, and allow quantitative predictions of particle geometry and flow parameters. Such calculations were made by Secomb & Gross (1983), extending those of Lin *et al.* (1973). The theory was shown to be appropriate at cell velocities above about 1 mm/s. Further results are presented here for several distinct classes of flexible particles (Özkaya 1985).

(*i*) *Long cylindrical particles.* This is the class of shapes to which the asymptotic solution in §4.2 applies. The indeterminate shape of the concave tail region is here modelled by a segment of a sphere, and the constraints of constant surface area and volume for a given cell are satisfied by adjusting the input parameters of the numerical integration (pressure drop, initial curvature and leakback). A sample set of results is shown in figure 3(*a*). Using this model, Secomb & Gross (1983) predicted values of apparent viscosity and tube haematocrit (Fahraeus effect) in good agreement with experimental results (Albrecht *et al.* 1979; Gaehtgens 1980; Lingard 1979) for blood flow in capillaries with diameters from 3 μm to 6 μm.

(*ii*) *Flared particles.* If the requirement that the membrane tension approach zero at the trailing end of the cell is relaxed, (4.1)–(4.4) allow solutions in which the cell shape is flared at the rear. The spherical segment used to approximate the membrane in the rear is then under uniform compression, and the pressure in the interior of the cell is greater than the upstream pressure. At the cusp, the tension in the outer membrane is in equilibrium with the compression in the spherical segment, but an additional constraint is implied, to prevent the membrane from moving around the rear rim, out of the region under compression. Also, the neglect of shear and bending forces in this limit means that the rear face cannot support a compressive stress, so this is not a realistic limiting shape for red-blood-cell shapes. Even so, a similar flare is obtained when bending resistance is taken into account (see below). A wide pressure swing in the lubrication layer is associated with the flaring of the trailing edge, as shown in figure 3(*b*).

(*iii*) *Bubble-shaped particles.* There is a lower limit (d_c) to the diameter of vessels through which a red blood cell may pass intact. To pass through vessels smaller than d_c requires an increase in the surface area of the cell, and haemolysis results if the increase is more than a few per cent. The critical diameter is calculated by assuming that the shape of the cell in a vessel of critical diameter is a cylinder with

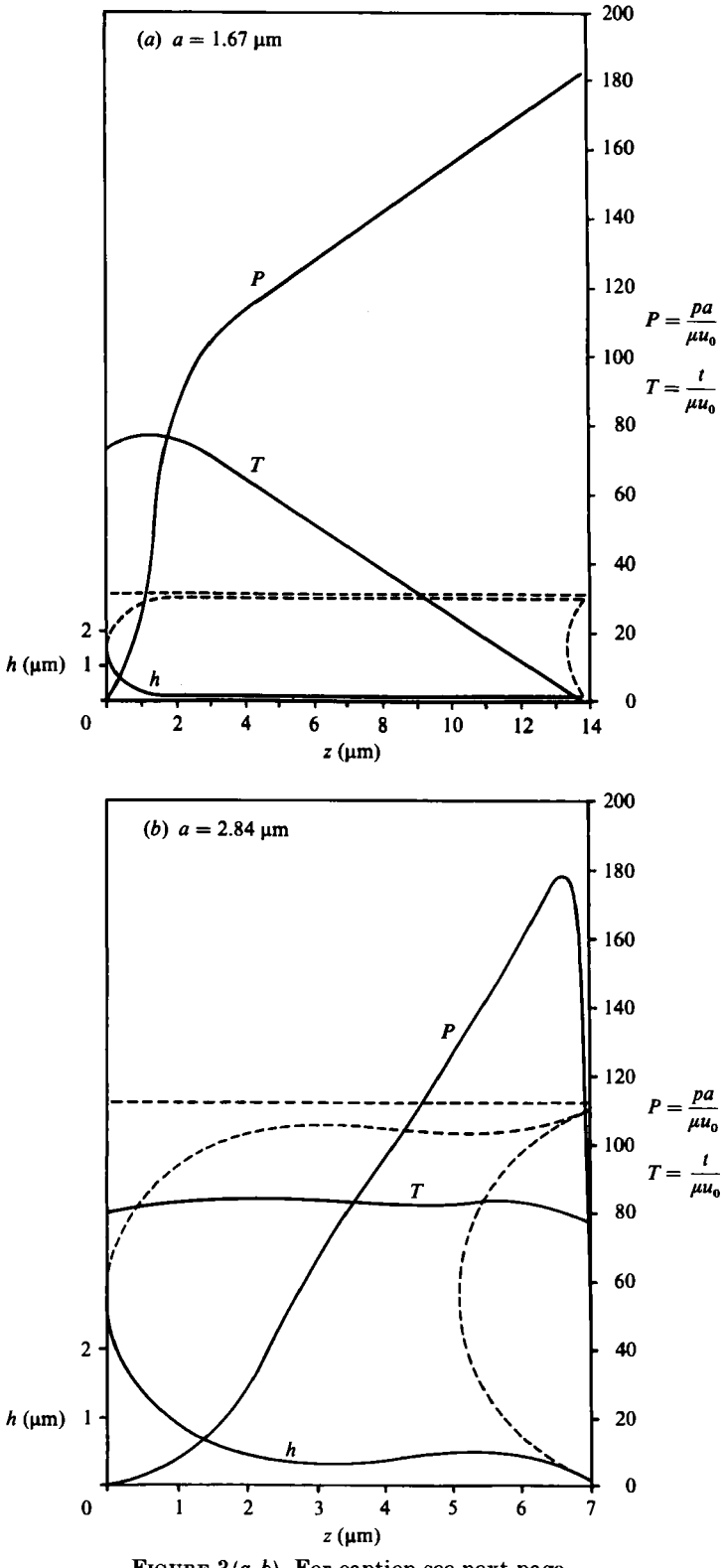

FIGURE 3(a,b). For caption see next page.

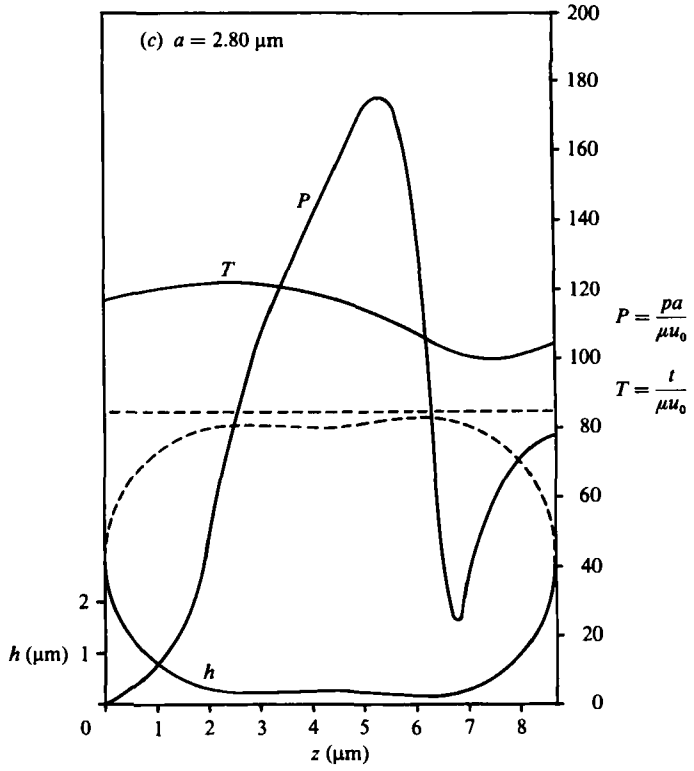

FIGURE 3. Cell shape, gap pressure and membrane tension calculated using the isotropic tension model for: (*a*) a long cylindrical particle; (*b*) a flared particle; (*c*) a bubble-shaped particle.

hemispherical ends (Canham & Burton 1968). If typical values for volume $V = 90\ \mu m^3$ and area $A = 135\ \mu m^2$ are assumed, then $d_c \simeq 2.8\ \mu m$.

A model for vessel diameters near 3 μm was developed by Secomb & Gross (1983). The cell was assumed to be effectively rigid with the critical shape already mentioned, and a simplified approximation to lubrication theory was used. The isotropic tension model provides a more detailed approach to this case. Equations (4.1)–(4.4) have solutions for bubble-like cell shapes without a cusp which are convex at both ends. An example is shown in figure 3(*c*), in which the surface area is that of a normal red blood cell but the volume is elevated.

5. Effects of membrane shear and bending resistance

The foregoing analysis shows that, as red-cell velocity falls, isotropic membrane tension decreases proportionally. Red-cell deformation remains finite, however, and so the elastic stresses resulting from membrane shear and bending are comparable to the isotropic tension at low enough velocities. The isotropic-tension model is then no longer appropriate, and cell shape and rheological properties become dependent on flow rate.

The effects of membrane shear elasticity, in the absence of bending rigidity, may be included by setting $\kappa > 0$ in (4.1)–(4.4). The non-dimensional parameter $\kappa/\mu u_0$ indicates the relative importance of shear elasticity. Resulting computed cell shapes are shown in figure 4. The tension t_s at the trailing edge is zero, as is the pressure drop

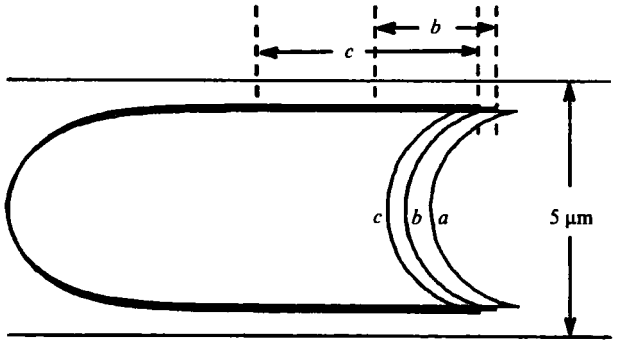

FIGURE 4. Cell shapes calculated including membrane shear but neglecting bending. (*a*) $u_0 \to 0$ (the isotropic tension limit); (*b*) $u_0 = 0.25$ cm/s; (*c*) $u_0 = 0.125$ cm/s. Regions of negative circumferential membrane tension are indicated at the top.

across the rear surface. Cusps are again present at the trailing edge, but the cell shape depends on the flow rate, the cell broadening with decreasing velocity. A region of negative circumferential tension ($t_\phi < 0$) is found to occur near the rear of the cell, in which the axisymmetric configuration is potentially unstable. Although buckling is to some extent inhibited by bending resistance, these results show the possibility of an inwardly buckled cleft whose length increases as the flow rate decreases. This qualitative behaviour is also shown in observations of red cells in capillaries by Hochmuth *et al.* (1970) and Gaehtgens, Dührssen & Albrecht (1980).

Both shear and bending elasticity are included in the studies of Zarda *et al.* (1977*a*) and Skalak & Tözeren (1980), who used finite elements to calculate the fluid flow and the cell shape in vessels of diameter 7.4 μm or more. In narrower vessels, the fluid gap becomes small and a lubrication theory approach is appropriate. To include shear and bending effects in a model based on lubrication theory, the boundary-value problem consisting of (3.5)–(3.10) and boundary conditions must be solved numerically.

The procedure is as follows. A new independent variable χ is introduced, representing the angular distance from the axis of a material element when the cell is inflated to a sphere of the same surface area. The computational domain is then fixed, namely $\{0 \leqslant \chi \leqslant \pi\}$. Equations (3.7)–(3.10) are singular on the axis, at $\chi = 0$ and $\chi = \pi$. The numerical solution is therefore obtained over a slightly reduced domain $\{\delta \leqslant \chi \leqslant \pi - \delta\}$ where $\delta = \frac{1}{50}\pi$, and matched to series solutions near the axis. For most parameter values of interest, the boundary-value problem is ill-conditioned, i.e. when integrated starting at one boundary it is very sensitive to initial values. Because of this, a 'multiple-shooting' routine is used (IMSL Inc., Houston, Texas). The domain is divided into 32 subdomains, separated by 'shooting points', and an iterative procedure is used. At each iteration, estimates of the independent variables at each shooting point are used as initial conditions to integrate over each subdomain. The estimates are then refined so as to improve the matching between solutions on adjacent subdomains. Convergence is generally achieved within a few iterations. However, for the smaller vessel diameters examined, and at very low or very high cell velocities, the solution is highly sensitive to the initial conditions even when integrated over small subdomains, and this limits the range of parameter values over which convergence could be achieved.

Cell shapes computed by this method are shown in figure 5, for a range of vessel diameters and cell velocities and other parameters as follows: $\mu = 1$ cP;

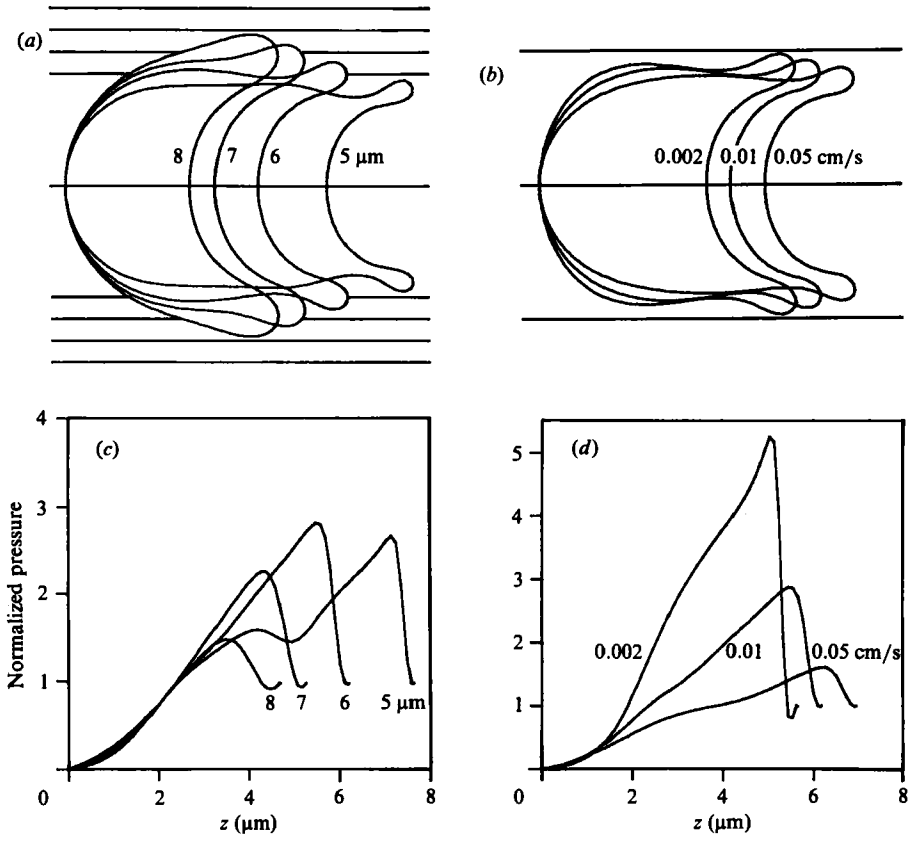

FIGURE 5. Cell shapes calculated including both shear and bending elasticity. (*a*) Cell velocity 0.01 cm/s, vessel diameters as shown. (*b*) Vessel diameter 6 μm, cell velocities as shown. (*c*, *d*) Variation of normalized pressure in the gap corresponding to cell shapes in (*a*) and (*b*).

$\kappa = 0.0042$ dyn cm; and $B = 1.8 \times 10^{-12}$ dyn cm. These computed shapes are consistent with those obtained using the simpler models and finite-element results of Skalak & Tözeren (1980) in that they show a rounded nose and a concave rear. Because bending resistance is included, the cusp at the trailing edge is replaced with a rim of finite curvature. The rim bulges outwards, and the minimum gap width is associated with this trailing edge, as observed experimentally by Bagge *et al.* (1980) and Gaehtgens *et al.* (1980).

The variation of pressure in the lubrication layer, normalized relative to the overall pressure drop, is also shown in figure 5. The outward bulge at the trailing edge produces a swing in pressure, as with the flared particles of §4.3. The amplitude of this swing decreases as cell velocity increases (figure 5*d*), suggesting the approach to the monotonic pressure profile shown in figure 3(*a*). The numerical scheme failed to converge at higher cell velocities, so a close approach to the high-velocity limit could not be demonstrated.

In a vessel of given diameter, the cells become broader as velocity decreases. Such changes in cell shape result in changes in apparent viscosity, which increases as flow rate decreases. Predictions of apparent intrinsic viscosity K_T over a wide range of cell velocities are shown in figure 6. The approach to the high-velocity limit is shown by the computations including shear but not bending elasticity. At cell velocities

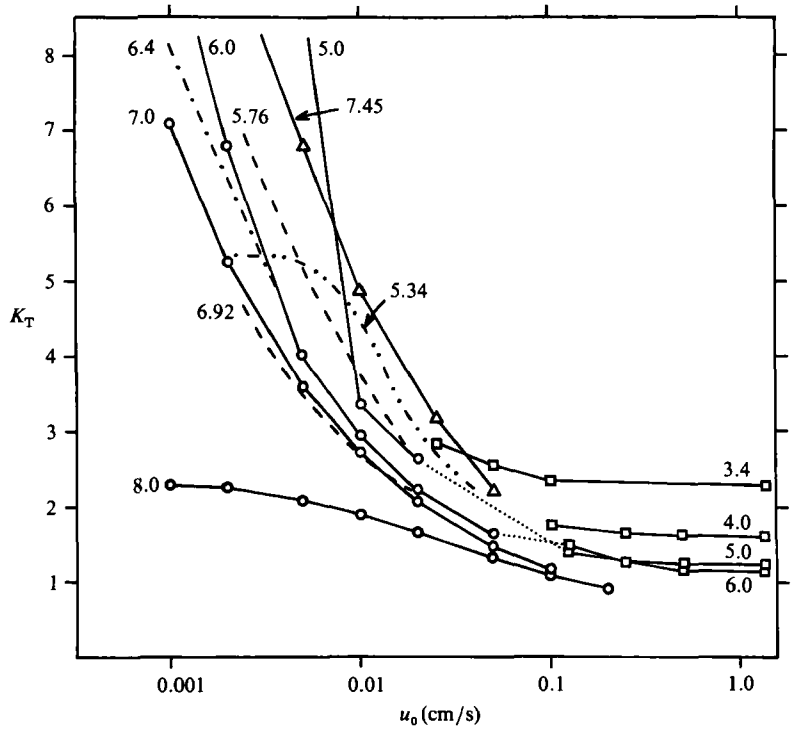

FIGURE 6. Variation of K_T with cell velocity u_0: comparison of present study with other theoretical and experimental studies. Vessel diameter in μm is shown on each curve. Theoretical results: □, lubrication model including shear elasticity but neglecting bending; ○, lubrication model including both shear and bending elasticity; △, finite-element results of Tözeren & Skalak (1980). Experimental results: – – – –, results of Lee & Fung (1969) using macroscopic model cells; ·· –· – ··, results of Lingard (1979) using human red blood cells; · –· –· –, results of Driessen *et al.* (1984) using rat red blood cells.

around 1 mm/s there is a small but significant increase in apparent viscosity from the asymptotic value. For vessel diameters of 5 μm and 6 μm, calculations have been made using both models (with and without bending), and the results appear to be consistent. Apparent viscosity rises rapidly at low velocities and is substantially higher at cell velocities 0.01 cm/s and below. The broadening of the cell at low velocities also leads to a decrease in the Fahraeus effect (H_T/H_D nearer to unity) as shown in figure 7.

6. Discussion

The experimentally measured bulk viscosity of whole blood corresponds to a value of K_T of at least 7.0. Our results thus confirm the marked reduction in the apparent viscosity of blood in capillaries (the Fahraeus–Lindqvist effect), over a wide range of flow rates. The dependence of K_T on flow rate is physiologically important since there is a very wide range of flow rates in the capillaries of a resting tissue, with many at or near stasis. Results of several experimental studies demonstrating this effect are included in figure 6. Driessen *et al.* (1984) studied rat red blood cells flowing through 6.4 μm glass capillary tubes, while Lingard (1979) passed human red cell suspensions through arrays of capillaries of diameter 5.34 μm. Lee & Fung (1969) used

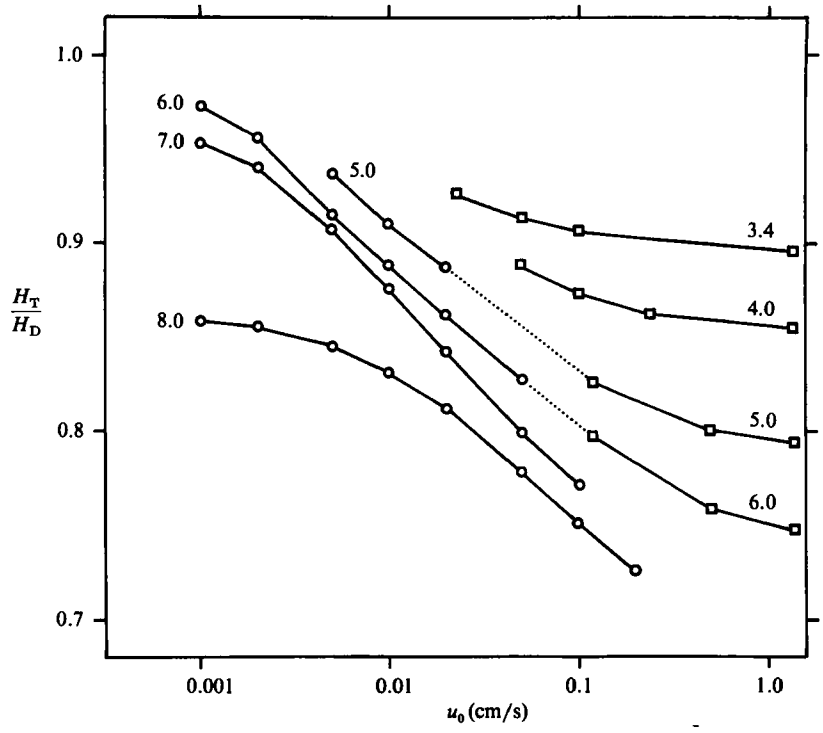

FIGURE 7. Variation of the Fahraeus effect, indicated by H_T/H_D, with cell velocity u_0: □, model including shear elasticity but neglecting bending; ○, model including both shear and bending elasticity.

rubber model cells in their study. In plotting their data, we have rescaled vessel diameters according to cell dimensions, and velocities via the dimensionless group $\mu u_0/M$, where M is the membrane elastic modulus for uniaxial in-plane stress. The lubrication-theory model shows satisfactory agreement with all these studies. Flexible model cells were also used by Sutera *et al.* (1970), under conditions corresponding to extremely low red-cell velocities.

At low cell velocities, the assumption about the unstressed shape of the red-blood-cell membrane becomes increasingly significant. Use of an axisymmetric model requires that the unstressed shape is axisymmetric and coaxial with the vessel. In fact, observations of red cells in narrow capillaries generally show that the axis of the biconcave disc lies perpendicular to the vessel axis, leading to the so-called 'crepe-suzette' shape in which the cell is folded over on itself. In our calculations, it is assumed that the membrane is unstressed in an inflated spherical shape, so that there is no preferred orientation. A cell with this property has more than one possible shape when freely suspended with normal volume. The results for vessel diameter 8 μm in figures 6 and 7 reflect an asymptotic approach at low velocities to a freely suspended, cupped shape with diameter slightly more than 7 μ. By contrast, Skalak & Tözeren (1980) assumed the unstressed cell shape to be a biconcave disc coaxial with the vessel. Their predicted values of intrinsic viscosity K_T are relatively high compared to the other data, probably because of this assumption. Other unstressed shapes may be modelled using the present lubrication theory approach, by including an additional term in (3.7) to represent the initial curvature.

In-vivo cell shapes in capillaries are generally not axisymmetric, but as yet there

have been few efforts at modelling asymmetric cell shapes. Secomb & Skalak (1982) used a two-dimensional model and predicted the occurrence of tank-treading (cf. Gaehtgens & Schmid-Schönbein 1982), and a reduced apparent viscosity for asymmetric cell shapes compared to corresponding symmetric shapes. It is not known whether non-axisymmetry produces a similar effect in a cylindrical capillary.

The overall aim of the studies reported here has been to understand the rheology of blood in terms of the mechanical properties of individual red blood cells. Axisymmetric models provide useful insights into several aspects of single-file flow in narrow capillaries. However, much work is required to achieve similar progress in understanding non-symmetric and complex multi-file flow in larger microvessels.

This work was supported by N.I.H. Grants HL17421, HL16851 and HL34555.

REFERENCES

Albrecht, K. H., Gaehtgens, P., Pries, A. & Heuser, M. 1979 The Fahraeus effect in narrow capillaries (i.d. 3.3 to 11.0 μm). *Microvasc. Res.* **18**, 33–47.

Bagge, U., Branemark, P.-I., Karlsson, R. & Skalak, R. 1980 Three-dimensional observations of red blood cell deformation in capillaries. *Blood Cells* **6**, 231–237.

Barnard, A. C. L., Lopez, L. & Hellums, J. D. 1968 Basic theory of blood flow in capillaries. *Microvasc. Res.* **1**, 23–34.

Bretherton, F. P. 1961 The motion of long bubbles in tubes. *J. Fluid Mech.* **10**, 166–188.

Canham, P. B. & Burton, A. C. 1968 Distribution of size and shape in populations of normal human red blood cells. *Circulation Res.* **22**, 405–422.

Chien, S., Sung, K.-L. P., Skalak, R., Usami, S. & Tözeren, A. 1978 Theoretical and experimental studies on viscoelastic properties of erythrocyte membrane. *Biophys. J.* **24**, 463–487.

Driessen, G. K., Fischer, T. M., Haest, C. W. M., Inhoffen, W. & Schmid-Schönbein, H. 1984 Flow behaviour of rigid red blood cells in the microcirculation. *Intl J. Microcirc. Clin. Exp.* **3**, 197–210.

Evans, E. A. & Skalak, R. 1980 *Mechanics and Thermodynamics of Biomembranes.* Boca Raton, Florida: CRC.

Evans, E. A. 1983 Bending elastic modulus of red blood cell membrane derived from buckling instability in micropipet aspiration tests. *Biophys. J.* **43**, 27–30.

Fischer, T. M., Stöhr-Liesen, M., Secomb, T. W. & Schmid-Schönbein, H. 1981*a* Does the dimple of the human red cell have a stable position on the membrane? *Biorheology* **18**, 46–47.

Fischer, T. M., Haest, C. W. M., Stöhr-Liesen, M. & Schmid-Schönbein, H. 1981*b* The stress-free shape of the red blood cell membrane. *Biophys. J.* **34**, 409–422.

Fitz-Gerald, J. M. 1969 Mechanics of red-cell motion through very narrow capillaries. *Proc. R. Soc. Lond.* B **174**, 193–227.

Gaehtgens, P. 1980 Flow of blood through narrow capillaries: Rheological mechanisms determining capillary hematocrit and apparent viscosity. *Biorheology* **17**, 183–189.

Gaehtgens, P., Dührssen, C. & Albrecht, K. H. 1980 Motion, deformation and interaction of blood cells and plasma during flow through narrow capillary tubes. *Blood cells* **6**, 799–812.

Gaehtgens, P. & Schmid-Schönbein, H. 1982 Mechanisms of dynamic flow adaptation of mammalian erythrocytes. *Naturwissenschaften* **69**, 294–296.

Gross, J. F. & Aroesty, J. 1972 Mathematical models of capillary flow: A critical review. *Biorheology* **9**, 225–264.

Gupta, B. B., Nigam, K. M. & Jaffrin, M. Y. 1982 A three-layer semi-empirical model for flow of blood and other particulate suspensions though narrow tubes. *J. Biomech. Eng.* **104**, 129–135.

Hochmuth, R. M., Marple, R. N. & Sutera, S. P. 1970 Capillary blood flow I. Erythrocyte deformation in glass capillaries. *Microvasc. Res.* **2**, 409–419.

LEE, J. S. & FUNG, Y. C. 1969 Modeling experiments of a single red blood cell moving in a capillary blood vessel. *Microvasc. Res.* **1**, 221–243.

LEW, H. S & FUNG, Y. C 1969 The motion of the plasma between the red blood cells in the bolus flow. *Biorheology* **6**, 109–119.

LIGHTHILL, M. J. 1968 Pressure-forcing of tightly fitting pellets along fluid-filled elastic tubes. *J. Fluid Mech*, **34**, 113–143.

LIN, K. L., LOPEZ, L. & HELLUMS, J. D. 1973 Blood flow in capillaries. *Microvasc. Res.* **5**, 7–19.

LINGARD, P. 1979 Capillary pore rheology of erythrocytes V. The glass capillary array-effect of velocity and hematocrit in long bore tubes. *Microvasc. Res.* **17**, 272–289.

LOMEN, D. O. & GROSS, J. F. 1977 A mathematical model of the effect of oxygen consumption on the resistance to the flow of sickle cell blood in capillaries. *Math. Biosciences* **37**, 63–79.

ÖZKAYA, N. 1985 Viscous flow of particles in tubes: Lubrication theory and finite element models. Ph.D. thesis, Columbia University, New York.

PAPENFUSS, H.-D. & GROSS, J. F. 1982 Mathematical model of the single-file flow of red blood cells in capillaries. In *Recent Contributions to Fluid Mechanics* (ed. W. Haase), pp. 180–195. Springer.

SECOMB, T. W. & GROSS, J. F. 1983 Flow of red blood cells in narrow capillaries: role of membrane tension. *Int. J. Microcirc. Clin. Exp.* **2**, 229–240.

SECOMB, T. W. & SKALAK, R. 1982 A two-dimensional model for capillary flow of an asymmetric cell. *Microvasc. Res.* **24**, 194–203.

SKALAK, R. 1976 Rheology of red blood cell membrane. In *Microcirculation*, vol. I (ed. J. Grayson & W. Zingg), pp. 53–70. Plenum.

SKALAK, R. & TÖZEREN, H. 1980 Flow mechanics in the microcirculation. In *Mathematics of Microcirculation Phenomena* (ed. J. F. Gross & A. Popel), pp. 17–40. Raven.

SUTERA, S. P., SESHADRI, V., CROCE, P. A. & HOCHMUTH, R. M. 1970 Capillary blood flow II. Deformable model cells in tube flow. *Microvasc. Res.* **2**, 420–433.

THOMAS, H. W. 1962 The wall effect in capillary instruments: An improved analysis suitable for application to blood and other particulate suspensions. *Biorheology* **1**, 41–56.

TIMOSHENKO, S. 1940 *Theory of Plates and Shells*. McGraw-Hill.

TÖZEREN, H. & SKALAK, R. 1978 The steady flow of closely fitting incompressible elastic spheres in a tube. *J. Fluid Mech.* **87**, 1–16.

TÖZEREN, H. & SKALAK, R. 1979 Flow of elastic compressible spheres in tubes. *J. Fluid Mech.* **95**, 743–760.

VANN, P. G. & FITZ-GERALD, J. M. 1982 Flow mechanics of red cell trains in very narrow capillaries. I. Trains of uniform cells. *Microvasc. Res.* **24**, 296–313.

WANG, H. & SKALAK, R. 1969 Viscous flow in a cylindrical tube containing a line of spherical particles. *J. Fluid Mech.* **38**, 75–96.

WHITMORE, R. L. 1968 *Rheology of the Circulation*. Pergamon.

ZARDA, P. R., CHIEN, S. & SKALAK, R. 1977*a* Interaction of viscous incompressible fluid with an elastic body. In *Computational Methods for Fluid–Solid Interaction Problems* (ed. T. Belytschko & T. L. Geers), pp. 65–82. New York: American Society of Mechanical Engineers.

ZARDA, P. R., CHIEN, S. & SKALAK, R. 1977*b* Elastic deformations of red blood cells. *Biorheology* **10**, 211–221.